JOURNAL OF APPLIED CRYSTALLOGRAPHY
ISSN 1600-5767

Quantitative phase analysis and microstructural characterization of urinary tract calculi with X-ray diffraction Rietveld analysis on a Caribbean island

Jaimie Greasley,[a]* Shivan Goolcharan[b] and Roger Andrews[a]

[a]University of the West Indies, St Augustine, Trinidad and Tobago, and [b]Eric Williams Medical Sciences Complex, Mount Hope, Trinidad and Tobago. *Correspondence e-mail: jaimie.greasley@gmail.com

Received 3 August 2021
Accepted 3 November 2021

Edited by J. Hajdu, Uppsala University, Sweden, and The European Extreme Light Infrastucture, Czech Republic

Keywords: kidney stone analysis; X-ray diffraction; quantitative Rietveld analysis; kidney stone composition; urolithiasis.

Supporting information: this article has supporting information at journals.iucr.org/j

In the twin-island state of Trinidad and Tobago, urinary stone analysis is not routinely performed. This study investigates, via powder X-ray diffraction, 52 urinary tract calculi collected from hospitals in Trinidad. Of these, 46 stones were analysed with Rietveld refinement for quantitative analysis and materials characterization. Refined unit-cell, microstructural and weight fraction parameters were obtained, with the last being used for stone classification. The results revealed seven distinct mineralogical phases of varying frequency: calcium oxalate monohydrate (COM, 58%), calcium oxalate dihydrate (COD, 23%), carbonated apatite (APA, 48%), brushite (BRU, 6%), struvite (STR, 42%), uric acid (UA, 23%) and ammonium acid urate (AAU, 19%). The average refined crystallite sizes were 1352 ± 90 Å (COM), 1921 ± 285 Å (COD), 83 ± 5 Å (APA), 1172 ± 9 Å (BRU), 1843 ± 138 Å (STR), 981 ± 87 Å (UA) and 292 ± 83 Å (AAU). Subsequently, 36.5% of stones were categorized as phosphates, 34.6% as oxalates, 13.5% as uric acid/urates and 15.4% as mixed compositions. The study findings highlight the importance of stone analysis as a necessary step towards disease management of local patients, and endorse the application of Rietveld refinement as a natural extension to diffraction-based kidney stone investigations.

1. Introduction

Urolithiasis, the pathological formation of concretions in the urinary tract, is an affliction suffered by many around the globe. It is the third most common urological disorder (Prezioso *et al.*, 2014), with a risk of 1–19% for Asian populations, 5–9% for Europeans and 12–15% for North Americans (Liu *et al.*, 2018; Ramello *et al.*, 2001). Epidemiological data depict a globally increased incidence of urolithiasis over the past few decades (Yoshida *et al.*, 1999; Hesse *et al.*, 2003; Stamatelou *et al.*, 2003; Sharma & Filler, 2010). Despite a patient being rendered stone free after medical and surgical interventions, there is also the issue of recurrence (Williams, 1963). Urolithiasis may bring about acute renal failure as a complication of urinary obstruction and/or inflammation of the kidney (Jamal & Ramzan, 2004; Keddis & Rule, 2013; Tang & Lieske, 2014). Recurrent stone formers are thus vulnerable to decreased renal function (Gillen *et al.*, 2005), the development of chronic kidney disease (CKD) and end-stage renal failure (ESRF) (Rule *et al.*, 2011; Kartha *et al.*, 2012; Keddis & Rule, 2013). Other concomitant associations include hypertension (Madore *et al.*, 1998), sepsis (Al-Mamari, 2017), osteoporosis (Pfau & Knauf, 2016) and urothelial carcinoma (Sun *et al.*, 2013).

Urinary tract calculi are due to the emergence, growth and clustering of mineralogical crystals in urine. Kidney stones are mostly crystalline, but are held together by a complex organic

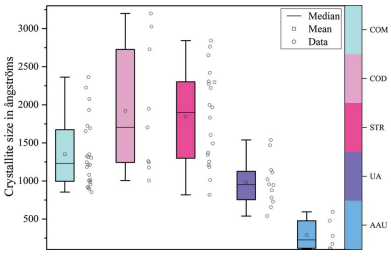

matrix comprising proteins and lipids (Khan & Kok, 2004; Khan *et al.*, 2016). Although it is reported that more than 100 different chemical species have been detected in kidney stones (Daudon & Jungers, 2012), only about a dozen of these are found in greater than 1% of cases. The most common minerals are calcium-based oxalates (CaOx) and phosphates (CaPh) (Daudon *et al.*, 2009). Non-calcareous minerals include magnesium phosphates, uric acid/urates, and, exceptionally, rare protein and drug-related compositions (Daudon *et al.*, 2016).

Calcium oxalate monohydrate (COM, $CaC_2O_4{\cdot}H2O$) or whewellite is by far the most frequent composition (Schubert, 2006). Its structure has been found in the monoclinic space group $P2_1/c$ (a = 6.316, b = 14.541, c = 10.116 Å, β = 109°). Calcium oxalate dihydrate (COD, $CaC_2O_4{\cdot}2H_2O$), called weddellite, is the less chemically stable oxalate form and converts to COM over time (He *et al.*, 2010; Izatulina *et al.*, 2018). It crystallizes in the tetragonal system with space group $I4/m$ (a = 12.371, c = 7.357 Å). CaOx stones tend to be ambiguous with regard to their aetiology. Elevated levels of oxalate and calcium ions in the urine, referred to medically as hyperoxaluria and hypercalciuria, respectively, are associated with their formation. However, these conditions in turn require further assessment as they arise from a multitude of possible metabolic, dietary or genetic influences (Pak, 1998; Moe, 2006).

Calcium phosphates include carbonated hydroxyapatite (APA, $Ca_5[PO_4,CO_3]_3OH$) and calcium hydrogen phosphate dihydrate or brushite (BRU, $CaHPO_4{\cdot}2H_2O$). Hydroxyapatite's structure belongs to the hexagonal $P6_3/m$ space group (a = 9.424, c = 6.879 Å), whereas brushite has been assigned to monoclinic space group Cc (a = 5.8105, b = 15.1758, c = 6.2337 Å, β = 116.405°). The latter phase is rare, but its presence in calculi signals severe stone disease (Klee *et al.*, 1991; Evan *et al.*, 2005).

Magnesium ammonium phosphate hexahydrate or struvite (STR, $MgNH_4PO_4{\cdot}6H_2O$) is more prevalent than the monohydrate form. It is orthorhombic, belonging to space group $Pmn2_1$ (a = 6.941, b = 6.137, c = 11.199 Å). Struvite stones arise from bacterial infection of urine. The production of urease, by specific strains of bacteria, facilitates the breakdown of urea into ammonia and carbon dioxide. This reaction alkalizes the urine and promotes the precipitation of struvite and carbonated apatite (Hess, 1990; Rahman *et al.*, 2003). Consequently, struvite and sometimes carbapatite stones are labelled as infection stones (Prywer & Torzewska, 2010).

Phases of uric acid and derivatives include anhydrous uric acid or uricite (UA, $C_5H_4N_4O_3$), uric acid dihydrate ($C_5H_4N_4O_3{\cdot}2H_2O$), ammonium acid urate (AAU, $C_5H_7N_5O_3$) and sodium urate ($C_5H_3N_4NaO_3$). Uricite belongs to space group $P2_1/a$ (a = 14.464, b = 7.403, c = 6.208 Å, β = 65°), and there is one hypothesized structural model for AAU which puts it in the triclinic space group $P\overline{1}$ (a = 3.65, b = 10.215, c = 10.597 Å, α = 113.9, β = 91.1, γ = 92.3°) (Friedel *et al.*, 2015). Uric acid requires consistently low pH urine for precipitation (Shekarriz & Stoller, 2002). Risk factors include gout or a family history of gout and a diet high in protein (Breslau *et al.*, 1988). Persons who are overweight, obese or diabetic have also been shown to be at risk for uric acid urolithiasis (Sakhaee *et al.*, 2002; Taylor *et al.*, 2005; Mosli *et al.*, 2013; Lieske *et al.*, 2006).

Multiple factors are implicated in stone formation. These may be classified as anatomical, genetic, metabolic, dietary or environmental in origin. Regardless of the aetiopathogenic forces at play, urinary stones are brought on by a specific set of physicochemical conditions and events. These are (i) the persistent supersaturation of the urine which leads to (ii) crystal nucleation and ultimately (iii) crystal growth and agglomeration (Finlayson, 1978). The first two circumstances are termed 'pre-requisites' as they produce crystals but do not compel the formation of a macroscopic stone (Rodgers, 2017). Urine is normally supersaturated with certain solutes and the appearance of crystals is not uncommon in non-stone formers (Grases *et al.*, 2000). What distinguishes lithogenic from normal urine is the frequency, size, morphology and extent of aggregation of the crystals (Kok *et al.*, 1990; He *et al.*, 2010).

1.1. Stone investigations

Kidney stones are proof of an atypical urinary environment, with appearance and crystalline composition being direct clues to their origin and development (Daudon *et al.*, 2008, 2016; Cloutier *et al.*, 2015). Analysis of stones should be a central component of diagnostic evaluation for all urolithiasis patients (Coe *et al.*, 1992; Grases *et al.*, 1998; Tiselius, 2000; Kourambas *et al.*, 2001). Knowledge of molecular composition is key to patients' risk evaluation for recurrent stone disease or more grave developments like CKD and ESRF. For this purpose, popular stone analysis techniques include wet chemical analysis, infrared spectroscopy (IR), scanning electron microscopy (SEM) and powder X-ray diffraction (PXRD) (Basiri *et al.*, 2012). PXRD and IR are the standard and recommended methods (Turk *et al.*, 2020).

Powder X-ray diffractometry permits the direct identification of crystalline phases due to the acquisition of characteristic diffraction patterns upon sample interaction with a monochromatic X-ray beam. Kidney stones are polycrystalline and may be effectively assessed via this technique. The inclusion of the Rietveld method for analysis of diffractograms helps to extract as much information as possible, other than simply stone composition (Le Bail *et al.*, 2008). A Rietveld procedure involves the iterative refinement of structural, microstructural and sample parameters such that a calculated profile becomes well fitted to the measured diffraction pattern. For kidney stone analysis, Rietveld studies have the potential to reveal structural details related to pathology-specific physicochemical conditions and stone growth mechanisms. In terms of microstructure, there are several indicators for further investigation into crystallite sizes of kidney stone phases (Shapur *et al.*, 2012; Daudon *et al.*, 2016; Bazin *et al.*, 2021).

This paper reports the analysis of urinary tract calculi in Trinidad using the powder X-ray diffraction method with Rietveld analysis. Our results are submitted in the form of weighted proportions of detected crystalline components for

each stone, the refined unit-cell dimensions and angles, and the crystallite size for each phase. Stones were classified on the basis of their quantitative composition. The data were analysed and compared with other batch stone studies conducted globally. The benefits of Rietveld studies for stone analysis are also discussed.

2. Experimental

2.1. Sample collection and preparation

Urinary tract calculi were collected from two public hospitals. The stones were rinsed with a saline solution post-removal and then stored in plastic or glass containers. Prior to analysis, the stones were rinsed again with de-ionized water and allowed to air-dry for up to 48 h. A ceramic mortar and pestle were used to grind the stones into a fine powder for XRD scanning.

2.2. Instrumentation and scanning

Diffraction scans were conducted with the Bruker D2 Phaser Tabletop X-ray diffractometer for the angular range $2 < 2\theta < 55^\circ$ with a 0.02° step size. The diffractometer setup was the standard Bragg–Brentano geometry with a primary and secondary goniometer radius of 141.4 mm. The radiation source was a ceramic X-ray tube with a Cu anode target. The wavelengths of $K\alpha_1$, $K\alpha_2$ and $K\beta$ were 1.5406, 1.5444 and 1.3922 Å, respectively, with a $K\alpha_2/K\alpha_1$ ratio of approximately 0.5. The optical system comprised 2.5° Soller modules, a 1 mm (0.6°) fixed divergence slit and an Ni $K\beta$ filter. The detector was a LynxEye linear position-sensitive detector.

2.3. Phase identification

Scan files were imported into the *DIFFRAC.EVA* software (Version 4.2; Bruker AXS GmbH, Karlsruhe, Germany). Crystalline phases were identified with the aid of the program's Search/Match operation using the ICDD PDF-2 (2011 version; International Centre for Diffraction Data, http://www.icdd.com) reference database. Phase presence was subsequently confirmed with Rietveld analysis.

2.4. Crystallite size and crystallinity

In *DIFFRAC.EVA*, the percent crystallinity of the samples was calculated with the `Crystallinity` function. This operation automatically determines the crystallinity according to equation (1),

$$\text{Crystallinity} = \left(1 - \frac{G - R}{G}\right) 100\%, \tag{1}$$

where G is the global area under the diffraction profile and R is the reduced area (area of Bragg peaks) after background subtraction.

Crystallite size calculations via the Scherrer method using both integral breadth (IB) and FWHM were performed on selected samples. The `Create Area` tool in *DIFFRAC.EVA* allows the user to demarcate the angular range of a single peak for crystallite size determination. Several single peaks were chosen from the scans and used for the *DIFFRAC.EVA* calculation. The instrumental contribution was set as the averaged FWHM of corundum peaks scanned using the same settings as the samples. The Scherrer constant k was provided as 1.

2.5. Rietveld refinement

The Rietveld method was first introduced in the 1960s (Rietveld, 1967, 1969) and is today adopted into numerous software programs (Le Bail *et al.*, 2008). The structure refinement routine involves the extraction of data from a calculated profile (I^{calc}) which has been fitted as well as possible to the observed data (I^{exp}) via minimization of the weighted sum of squares, WSS,

$$\text{WSS} = \sum_{i=1}^{N} w_i^2 \left(I_i^{\text{exp}} - I_i^{\text{calc}}\right)^2. \tag{2}$$

The calculated intensity at the ith point of a pattern (I_i^{calc}) is a sum over the contributions of all the phases, peaks and background at that point,

$$I_i^{\text{calc}} = \underbrace{I \sum_{j=1}^{N_{\text{phases}}} \frac{f_j}{V_j^2}}_{\text{scale factor}} \left[\sum_{k=1}^{N_{\text{peaks}}} L_k |F_{k,j}|^2 \underbrace{G_j(2\theta_i - 2\theta_{k,j})}_{\text{PSF}} P_{k,j} A_j \right] + \underbrace{\sum_{n=0}^{N_b} a_n (2\theta_i)^n}_{\text{bkg}}. \tag{3}$$

How well a calculated pattern matches the observed profile is ordinarily judged by means of the weighted profile R factor:

$$R_{\text{wp}} = \left[\frac{\text{WSS}}{\sum_{i=1}^{N} \left(w_i I_i^{\text{exp}}\right)^2} \right]^{1/2}. \tag{4}$$

The lower the value of R_{wp}, the better the fit is presumed to be.

In these equations, $w_i = 1/(I_i^{\text{exp}})^{1/2}$, I is the beam intensity, f_j is the phase volume fraction for the jth phase, V_j is the unit-cell volume of phase j, L_k is the Lorentz polarization factor of the kth peak, $|F_{k,j}|^2$ is the squared structure factor for the kth peak of the jth phase, G_j is the peak shape function (PSF) for phase j, $P_{k,j}$ is the preferred orientation correction for peak k in phase j, A_j is the X-ray absorption correction for phase j, a_n is the background (bkg) coefficient for the nth polynomial and N_b is the degree of polynomial for background modelling.

2.5.1. Phase quantification. For a multiphase sample, the weight fraction of the pth phase is computed by the simple relation in equation (5) (Hill & Howard, 1987). In Rietveld software, the scale factors and structural parameter values from the refinement are used to calculate these fractions.

$$W_p = \frac{S_p Z_p M_p V_p}{\sum_i S_i Z_i M_i V_i}, \tag{5}$$

where S is the Rietveld scale factor, Z is the number of formula units per unit cell, M is the mass per unit cell and V is the unit-cell volume.

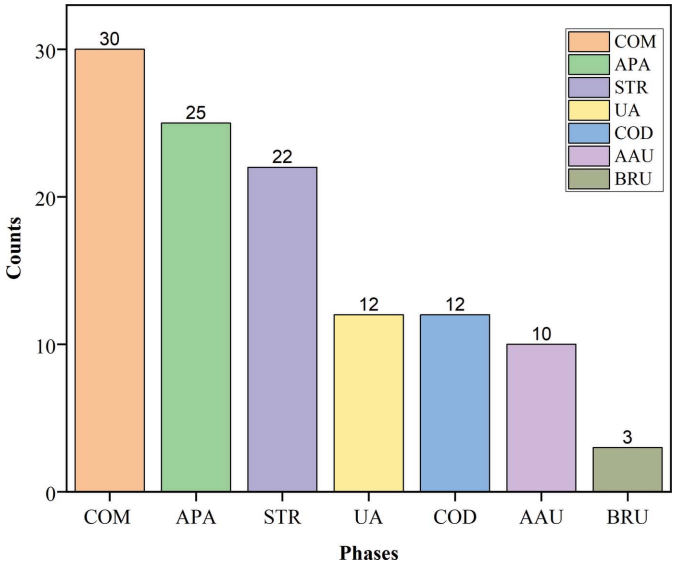

Figure 1
The frequency of crystalline phases across 52 stones.

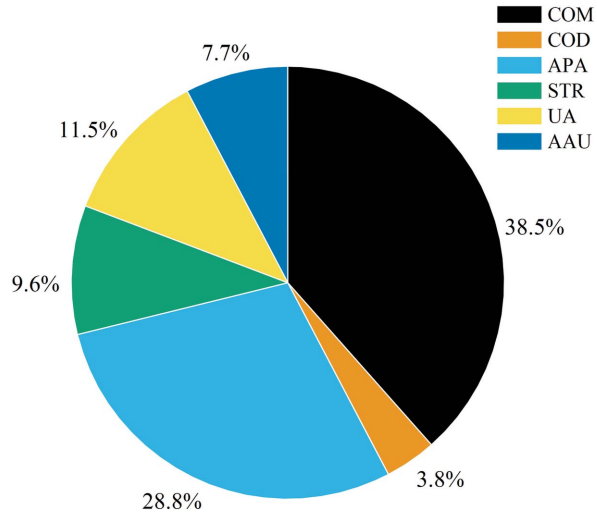

Figure 2
The relative abundance of the phase majorities.

2.5.2. *MAUD* analysis. The refinements were performed in *Materials Analysis Using Diffraction* (*MAUD*) (Lutterotti *et al.*, 1999). The software features classic optimization algorithms for quantitative phase analysis and microstructural and texture analysis for materials characterization from X-ray, neutron and electron diffraction data. Structural data for detected phases were imported as CIFs from the Crystallography Open Database (Gražulis *et al.*, 2009) for COM (ID 2300210; Daudon *et al.*, 2009), COD (ID 9000764; Tazzoli & Domeneghetti, 1980), APA (ID 9011094; Sudarsanan & Young, 1969), BRU (ID 9007305; Schofield *et al.*, 2004), STR (ID 2106462; Whitaker & Jeffery, 1970) and UA (ID 9011061; Ringertz, 1966). The structural data for AAU (Friedel *et al.*, 2015) were registered manually into *MAUD*.

A typical procedure involves step-wise refinement of the following parameters: (i) background and scale, (ii) zero offset, unit-cell lengths and angles, and displacement parameters, (iii) crystallite size and microstrain, and (iv) preferred orientation. For crystallite size modelling in *MAUD*, anisotropic line broadening was chosen. Crystallite sizes were started at 1000 Å for most phases, except APA and AAU which were started at 100 and 500 Å, respectively. The general spherical harmonics model was applied to accommodate preferred orientation.

3. Results and discussion

3.1. Phase composition

Phase identification revealed seven distinct crystalline phases, which were COM, COD, hydroxyapatite/carbapatite (APA), BRU, STR, UA and AAU. There was no attempt made to distinguish hydroxyapatite from carbapatite as biological apatites are always carbonated to some degree (Maurice-Estepa *et al.*, 1999; Bazin *et al.*, 2009). There were between one and four phases in each stone, with a modal value of two phases per stone. Thirteen were monophasic, 23 were biphasic, nine had three phases and seven had four phases. It was more likely that a stone comprised more than one phase, which is in accordance with the findings of Schubert (2006).

The bar chart in Fig. 1 depicts the number of calculi found to contain the seven phases. COM was the most abundant mineral, having been discovered in 30 of 52 stones. This was followed by APA ($N = 25$), STR ($N = 22$), UA ($N = 12$), COD ($N = 12$) and AAU ($N = 10$), and the least common was BRU ($N = 3$). All phases, with the exception of the last, were detected as majority constituents in at least one stone (Fig. 2). Here, we define 'majority' as containing a weight fraction more than or equal to half. Pure (monophasic) stones were observed for COM, APA, STR and UA, but no pure AAU or COD stones were found.

3.2. Phase correlation

With respect to the co-existence of two given phases within a stone, Pearson correlation co-efficients were computed. The colour matrix is depicted in Fig. 3, with shades of blue indicating positive correlation ($r > 0$) and red indicating a negative correlation ($r < 0$) between a phase pair. Correlations deemed significant ($p \leq 0.01$) are labelled within colour blocks. A significant positive covariance was found between COM and COD ($r = 0.469, p < 0.001$), APA and STR ($r = 0.500, p < 0.001$), and UA and AAU ($r = 0.428$, $p = 0.002$). Significant negative covariances were found for COM and STR ($r = -0.448$, $p < 0.001$), COD and STR ($r = -0.377$, $p = 0.006$), and APA and UA ($r = -0.527$, $p < 0.001$). Overall, these values indicate that oxalate, phosphate and uric acid phases are likely to be present alongside other phases of the same group, but the co-existence of two phases of different groups is unlikely. In the chemical context, this is logical as the conditions giving rise to specific phases may preclude others. It should be noteworthy when unlikely phases appear together, as this may signal crucial changes in urinary conditions and lithogenic contributors.

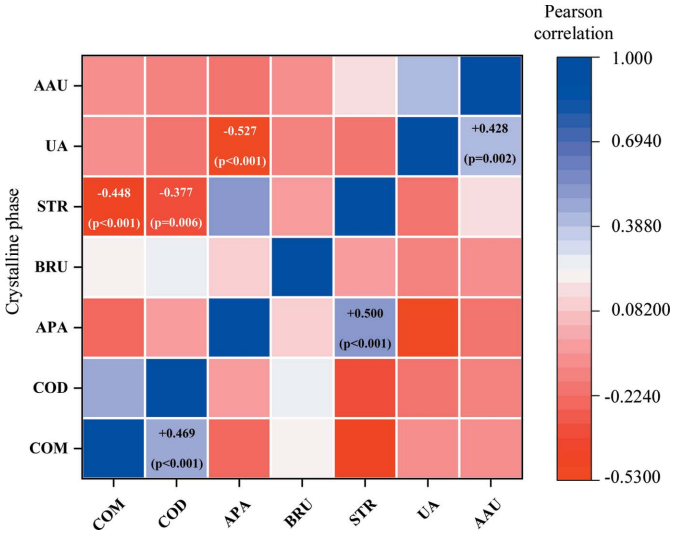

Figure 3
The relative abundance of the phase majorities.

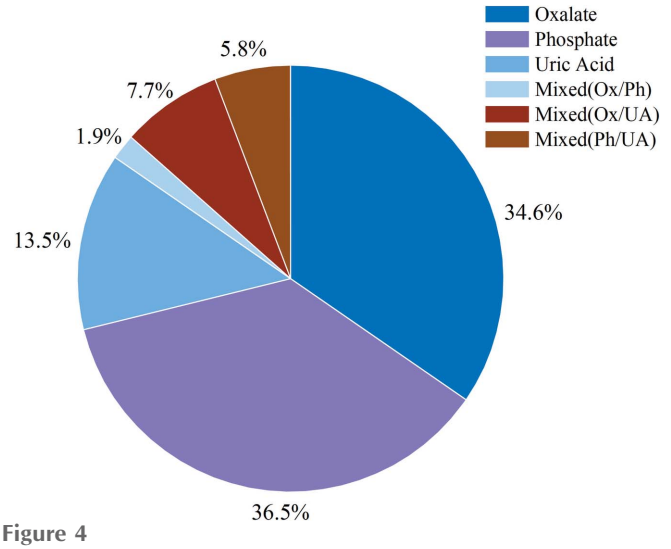

Figure 4
The abundance of stone categories and sub-categories.

3.3. Stone classification

Fifty-two urinary tract stones were analysed qualitatively for their composition. The majority, 46, were submitted to a complete Rietveld analysis. The remainder were only partially assessed because of difficulties in the refinement of multiple phases or an unsatisfactory R_{wp} factor due to inadequate modelling of strong preferred orientation. Nevertheless, preliminary quantitative results facilitated their classification. The stones fell into four major categories: oxalates, phosphates, uric acid/urates and mixed stones. There were no discovered protein or drug stones. A sample was categorized as an 'oxalate', 'phosphate' or 'uric acid/urate' if about 70% of its weight constituted phases belonging to the specified class. Calculi were deemed 'mixed' if there was a weight ratio of at least 3:2 of phases belonging to two distinct classes.

Our results show two major stone categories (phosphate and oxalate) and two minor categories (uric acid/urate and mixed). The relative abundance of each category is depicted in the pie chart in Fig. 4. The numbers of stones classified as oxalate, phosphate, uric acid/urate and mixed were 18, 19, seven and eight, respectively. Among oxalate stones, 59% consisted of solely oxalate phases, that is whewellite and weddellite. The rest were majority oxalate with some phosphate or uric acid/urate content. Pure whewellite stones represented 41% of all oxalates, but no pure weddellite stones were found. Within the phosphate group, 80% consisted of solely phosphate phases, mainly apatite and struvite, and the remainder contained trace amounts of whewellite. From the seven samples classified as uric acid/urate stones, two were pure uric acid stones, three were uric acid with ammonium acid urate and the rest contained small amounts of oxalate or phosphate phases. For the mixed stones category, half were a combination of oxalate and uric acid/urate phases, 38% were a combination of phosphate and uric acid/urate phases, and a single stone was a mixed oxalate/phosphate stone.

Chatterjee *et al.* (2018) reported a dominance of oxalate stones for eastern India on the basis of XRD data. From a nearly identical sample size of 50 stones to our 52, 82% were classified as oxalates, which is different from what we have reported. It is obvious from our data that whewellite was the most frequent phase (30/52). However, oxalate phases were the majority (wt% $\geq$ 50%) for just 42.3% (22/52), half the number reported by Chatterjee and co-workers. Moreover, our classification criterion for mixed calculi led to only 34.6% (18/52) being definitely 'oxalate' stones as substantial amounts of non-oxalate phases were also present.

A Japan-based study also showed a high dominance of stones consisting of oxalate, comparable to the reports of Chatterjee *et al.* (2018). Hossain *et al.* (2003) recorded 81.6% stones with CaOx, 15.8% uric acid/urate-containing stones and just 3.7% struvite stones via semi-quantitative IR spectroscopic analysis. An advantage of their analysis is a large sample size of more than 1800 stones, but the lack of a fully quantitative method and rigid classification protocol makes direct comparison difficult. In the current work, UA and AAU were also detected at a high frequency in 23.1 and 19.2% of stones, respectively.

Uvarov *et al.* (2011) gave figures of 43.2% oxalates, 35.9% mixed stones, 10.3% urates and 7.7% phosphates from a reference intensity ratio XRD assessment of 278 stones in Jerusalem. A high proportion of mixed stones is prominent from their results, but is most likely attributable to the absence of a quantitative boundary in the classification method. Our results give 15.4% for mixed calculi, though following the same approach would yield 40.4%, scaling similarly to their findings.

Giannossi *et al.* (2012) documented 59% oxalate stones followed by 18% uric acid from a batch of 80 stones in southern Italy using qualitative analysis with SEM, PXRD and optical microscopy. Ma *et al.* (2017) conducted an extensive qualitative analysis of 2437 stones with Fourier transform IR spectroscopy, of which 720 were imaged with SEM. They reported 53% oxalates, 18% uric acid and 6% total phosphates (APA, BRU, STR) for their hospital in Guangzhou. Keshavarzi *et al.* (2016) noted an abundance of whewellite and

uricite from XRD Rietveld analysis of 39 stones for Iran. Most of their data set were sole oxalates (28%) and uric acid (21%) or mixed oxalate–uric acid compositions (41%). The remainder were split up into isolated or double cases of cystine or pure or mixed oxalate–phosphates.

Some consistency is seen from the above reports: oxalates are most common, followed by uric acid and then phosphates. Our data deviate from this, as phosphates and oxalates are equally dominant. Similar findings of co-dominant oxalate and phosphate stones, 32 and 37%, respectively, were cited in a very recent study on a Mayan population in Mexico (Cruz-May *et al.*, 2021).

One variation amongst the previous reports is the wide gap between the dominant oxalate and uric acid groups outlined by Hossain *et al.* (2003) and Chatterjee *et al.* (2018) but not by the others, who report a lesser abundance of oxalates, greater frequency of other groups and a 'mixed' category. Our report also follows the trend of the latter.

Caution must be taken in making and interpreting these comparisons. Uvarov *et al.* (2011) highlighted the lack of a standard in classifying stones amongst studies, which is especially apparent in our discussion for 'mixed' calculi. The greatest uncertainty lies in differences in the analytical procedures used by stone researchers. Some surveys employed XRD as their principal technique, others IR. Some analyses are quantitative or semi-quantitative, with others relying on a qualitative assessment alone. Only Chatterjee *et al.* (2018) and Keshavarzi *et al.* (2016) employed Rietveld analysis in the above studies. Additionally, the sample size is quite varied, ranging from dozens of calculi to thousands. Whilst using more advanced methods, smaller studies like ours may not accurately represent the entire study population.

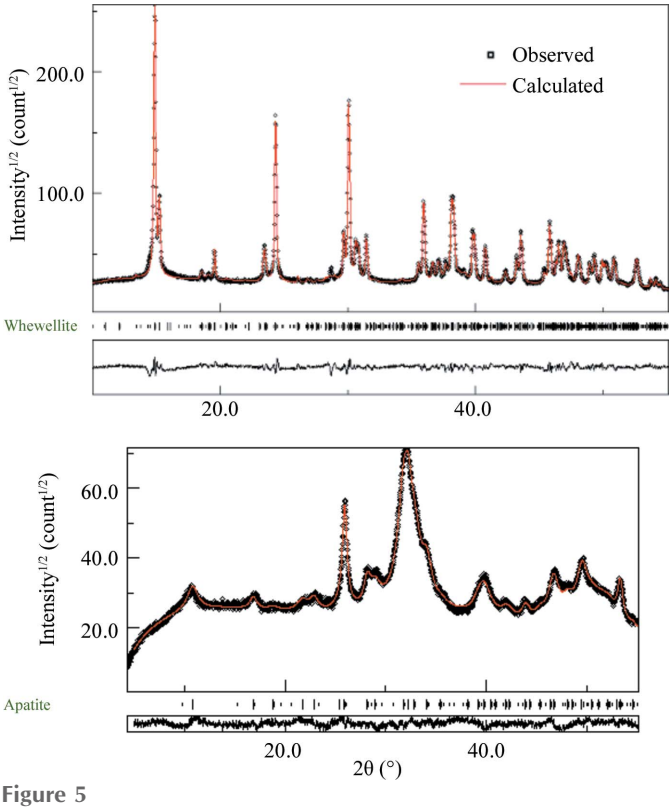

Figure 5
Rietveld refinement of whewellite sample C24 (top) and apatite sample C33 (bottom).

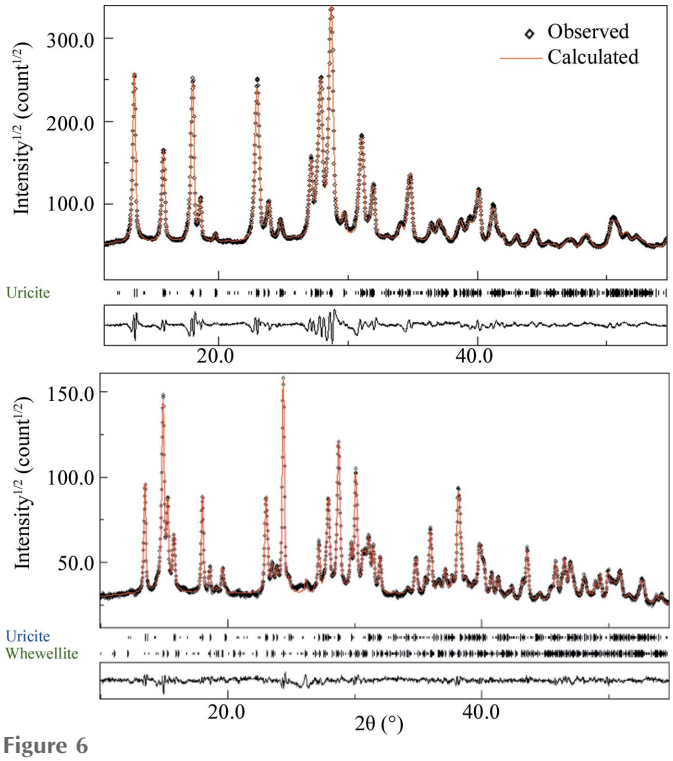

Figure 6
Rietveld refinement of monophasic sample C1 (top) and biphasic sample C46 (bottom).

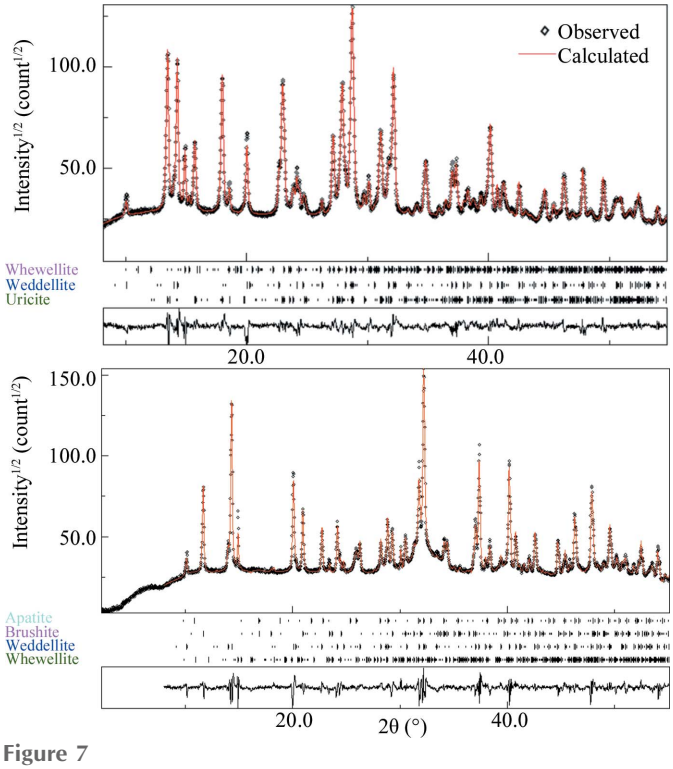

Figure 7
Rietveld refinement of triphasic sample C2 (top) and four-phase sample C9 (bottom).

Table 1
Composition, classification (Class.) and Rietveld refinement data for 46 urinary tract calculi.

The table shows refined values of unit-cell parameters, percentage weight (Wt%) and crystallite size (Crys.) for each identified phase alongside the weighted *R* factor (R_{wp}). Final stone classifications are labelled as oxalate (Ox), phosphate (Ph), uric acid/urate (Ur) and mixed (Mx).

					Cell dimensions (Å)			Cell angles (°)			
Label	R_{wp}	Class.	Phase	Wt%	*a*	*b*	*c*	*α*	*β*	*γ*	Crys. (Å)
C1	0.0859	Ur	UA	100	14.502	7.469	6.22		65.08		657
C2	0.0812	Ur	UA	74.7	14.497	7.457	6.215		64.99		729
			COD	22.2	12.399		7.37				1006
			COM	3.1	6.301	14.621	10.149		109.55		1323
C3	0.1045	Ph	APA	56.3	9.437		6.899				77
			STR	43.7	6.958	6.144	11.223				1371
C4	0.0986	Ox	COD	60.9	12.378		7.359				1704
			COM	39.1	6.294	14.595	10.124		109.42		1215
C5	0.0788	Ur	UA	61.4	14.482	7.459	6.214		65.05		539
			AAU	33.2	3.659	10.16	10.618	113.61	91.02	92.7	174
			STR	5.4	6.945	6.153	11.237				818
C6	0.0944	Ph	STR	51.3	6.949	6.139	11.217				1345
			APA	48.7	9.456		6.884				81
C7	0.0944	Ur	UA	100	14.511	7.473	6.226		65.06		781
C8	0.0959	Ph	STR	86.5	6.951	6.142	11.221				2307
			APA	13.5	9.401		6.91				67
C9	0.0998	Ox	COD	57.7	12.368		7.36				1244
			APA	21	9.437		6.875				67
			BRU	10.8	5.817	15.171	6.253		116.41		1163
			COM	10.5	6.211	14.564	10.164		107.08		1724
C10	0.083	Ox	COM	82.6	6.298	14.606	10.123		109.47		1303
			APA	15	9.416		6.89				94
			COD	2.5	12.36		7.36				1260
C11	0.0934	Ox	COM	80.8	6.298	14.604	10.124		109.46		2225
			APA	15.4	9.443		6.88				122
			COD	3.8	12.378		7.365				3027
C12	0.0549	Ph	APA	84.9	9.44		6.887				69
			STR	15.1	6.954	6.143	11.219				2420
C13	0.1031	Ox	COM	69.3	6.297	14.607	10.127		109.45		2075
			COD	30.7	12.378		7.361				1949
C14	0.0644	Ph	APA	58.9	9.48		6.887				60
			STR	41.1	6.957	6.14	11.216				2650
C15	0.078	Ox	COM	72.8	6.297	14.603	10.125		109.47		2364
			APA	25	9.446		6.885				147
			COD	2.2	12.368		7.364				1175
C16	0.0725	Ph	APA	71.3	9.447		6.883				67
			COM	14.1	6.302	14.61	10.129		109.47		1246
			STR	8.5	6.988	6.133	11.22				1832
			BRU	6.1	5.85	15.183	6.31		117.04		1180
C17	0.112	Ox	COM	100	6.296	14.607	10.126		109.46		5328
C18	0.0574	Ph	APA	81.3	9.431		6.885				84
			STR	18.7	6.947	6.136	11.22				2221
C19	0.075	Mx	APA	48.5	9.476		6.887				83
		(Ph/Ox)	COM	26.2	6.3	14.612	10.129		109.47		1933
			STR	13.6	6.955	6.14	11.225				1998
			COD	11.8	12.377		7.364				2728
C20	0.0595	Ph	APA	71	9.428		6.885				89
			COM	29	6.297	14.608	10.127		109.44		988
C21	0.075	Ox	COM	81.1	6.297	14.605	10.128		109.47		1184
			UA	18.9	14.472	7.473	6.205		65.04		1142

3.4. Rietveld analysis

Forty-six calculi underwent a complete Rietveld analysis with *MAUD*. The refined values of unit-cell parameters, percentage weight (Wt%) and crystallite size (Crys.) for each identified phase alongside the weighted *R* factor (R_{wp}) are listed in Table 1. The final stone classifications are also labelled in the table as oxalate, phosphate, uric acid/urate and mixed. Observed and calculated intensities for samples with one, two, three and four phases co-present are provided in Figs. 5–7. The entire collection of Rietveld plots is available as supporting information.

The final unit-cell parameters were generally quite similar to the starting values ($\Delta < 0.5\%$) with a few exceptions ($0.5 < \Delta < 2\%$). The greatest variations were observed for AAU. However, only six refinements were performed for this phase since its triclinic structure made refinement challenging. Deviations were also observed for some samples with minor phases, *e.g.* C9 for COM, C37 for APA, and C5, C16 and C45 for STR.

The crystallite size data are statistically summarized for each phase in Table 2, with the crystallite size distributions for the three most frequent phases illustrated in Fig. 8. Box plots for most phases are provided in Fig. 9. For COM, the distribution is right skewed. One outlier was omitted from the statistical calculations for a pure COM stone (C17). The diffractogram displayed extreme texture which was difficult to model, and the final crystallite size was 5328 Å. Apatite (APA) showed the smallest crystallite sizes and a positively skewed distribution. The lower bound of 25 Å (C37) is a possible outlier, as may be seen from Fig. 8. The second smallest value was 60 Å. Struvite revealed quite large crystallite sizes with the highest median value of 1899 Å (Table 2). The distribution appears bimodal at 1250 and 2250 Å. For other phases, the number of refinements performed was significantly lower. COD crystallites presented the widest range of values from $N = 9$ refinements and the largest mean size at 1921 ± 285 Å. The uric acid crystallites had mean and median sizes below 1000 Å. Ammonium acid urate had the second smallest sizes following apatite. Brushite was only refined twice and took values of 1160 and 1183 Å.

The sizes for COM, UA and AAU are quite similar to what has been published by Chatterjee *et al.* (2015, 2018). The APA

Table 1 (continued)

Label	R_{wp}	Class.	Phase	Wt%	Cell dimensions (Å)			Cell angles (°)			Crys. (Å)
					a	*b*	*c*	*α*	*β*	*γ*	
C22	0.0521	Ph	APA	88.5	9.436		6.875				76
			STR	11.5	6.941	6.131	11.211				1492
C23	0.1073	Ox	COM	100	6.299	14.613	10.13		109.48		1655
C24	0.0758	Ox	COM	100	6.299	14.608	10.124		109.45		1211
C25	0.0925	Ox	COM	100	6.301	14.612	10.131		109.47		1015
C26	0.081	Ox	COM	100	6.303	14.619	10.129		109.45		920
C27	0.0449	Ph	APA	64.1	9.426		6.895				80
			STR	35.9	6.951	6.14	11.214				1966
C28	0.0684	Ox	COM	74.3	6.3	14.608	10.124		109.45		1005
			COD	25.7	12.373		7.358				3199
C29	0.0578	Ph	APA	89.4	9.446		6.871				64
			STR	10.6	6.936	6.135	11.214				1013
C30	0.0743	Ur	UA	88.2	14.493	7.463	6.214		65.04		947
			AAU	11.8	3.69	10.12	10.671	113.6	90.15	91.93	117
C31	0.0669	Mx	COM	53.1	6.297	14.604	10.126		109.45		897
		(Ox/UA)	UA	37.6	14.473	7.455	6.204		65.01		1022
			STR	6.3	6.959	6.138	11.207				1604
			AAU	2.9	3.675	10.171	10.608	113.76	90.7	92.78	595
C32	0.0875	Ph	STR	100	6.952	6.14	11.223				2276
C33	0.051	Ph	APA	100	9.433		6.872				81
C34	0.0577	Ph	APA	100	9.452		6.864				69
C35	0.0731	Ur	AAU	58.7	3.669	10.094	10.656	113.46	90.81	93.02	478
			UA	41.3	14.53	7.444	6.252		64.6		880
C36	0.0544	Ph	APA	71.6	9.428		6.879				127
			COM	28.4	6.298	14.6	10.121		109.47		1350
C37	0.0866	Mx	AAU	50	3.675	10.076	10.661	113.52	90.75	92.54	280
		(Ph/UA)	STR	37.3	6.957	6.141	11.226				1208
			APA	12.7	9.51		6.89				25
C38	0.0666	Ph	APA	72	9.437		6.887				70
			STR	18.7	6.953	6.14	11.22				2763
			COM	9.3	6.296	14.608	10.125		109.47		1693
C39	0.0554	Ph	APA	61.5	9.439		6.884				75
			STR	38.5	6.949	6.138	11.215				2844
C40	0.0607	Ox	COM	100	6.301	14.61	10.127		109.45		908
C41	0.0815	Ox	COM	100	6.3	14.614	10.13		109.46		1316
C42	0.1175	Ph	STR	100	6.955	6.139	11.221				1253
C43	0.0689	Mx	COM	60.8	6.299	14.609	10.126		109.46		1080
		(Ox/UA)	UA	39.2	14.479	7.457	6.206		65.01		1539
C44	0.1088	Ph	STR	82.7	6.957	6.142	11.227				2297
			APA	17.3	9.428		6.87				124
C45	0.0691	Mx	COM	42.5	6.301	14.614	10.13		109.47		957
		(Ox/UA)	UA	38.3	14.486	7.458	6.206		65.01		957
			AAU	15.9	3.666	10.175	10.599	113.85	90.92	93.53	105
			STR	3.3	6.97	6.141	11.213				1185
C46	0.0516	Mx	COM	55	6.301	14.61	10.127		109.45		854
		(Ox/UA)	UA	45	14.48	7.459	6.206		65.02		1112

values are smaller in our study as most fell below 10 nm, whereas Chatterjee and co-workers reported a range of 10–35 nm. Conversely, a broader and larger range of crystallite sizes was obtained in our study for COD (101–320 nm) than theirs (42–167 nm) for the same number of refinements. There is a difference in methodology, however, as the anisotropic model was implemented in our refinements as opposed to the isotropic model for crystallite size modelling. Bazin *et al.* (2009) wrote that biological apatite nanocrystals in bone were about 10 nm, which matches well with our results. Bazin *et al.* (2012) measured a mean value of 250 nm for struvite crystals via powder neutron diffraction. In agreement, 40% of our values reflect a size greater than 200 nm and 60% above 150 nm for STR.

3.5. *DIFFRAC.EVA* analysis

3.5.1. Scherrer crystallite size. A handful of samples were analysed where possible with the traditional IB and FWHM approaches included in the *DIFFRAC.EVA* software (Table 3). The values were lower than the Rietveld-refined crystallite sizes by 33–70%, but the general order of the phases is maintained. The UA sizes were smaller than those of COM, which in turn were smaller than those of STR. Uvarov *et al.* (2011) also employed the FWHM method to evaluate crystallite sizes for hundreds of samples. Our findings correlate well with their modal values for COM and UA of 70 and 45 nm, respectively. Limitations of this method are the multi-phasic compositions of some samples and overlapping peaks, especially with APA, which make single peak area and width measurements difficult or even impossible. Only distinctly separated low-angle peaks were considered, which was remarkably limiting and not representative of all *hkl* peaks.

3.5.2. Crystallinity. The percent crystallinity averaged 56.3% across all samples. In ranking order of increasing crystallinity, the stone categories were phosphates (48.5% crystalline), mixed (54%), oxalates (61.9%) and uric acid stones (65.2%). These data are similar to the results of Mirković *et al.* (2020), who calculated high crystallinities for COM and COD of 68% and for UA of 65%, although our averages were based on stone type and not individual phases as in their study. The phosphate category ranked

Table 2
Summary of Rietveld refinement crystallite size data.

Phase	No. of refinements	Range (Å)	Median (Å)	Mean (Å)
COM	24	854–2364	1231	1352 ± 90
COD	9	1006–3199	1704	1921 ± 285
APA	23	25–147	77	83 ± 5
STR	20	818–2844	1899	1843 ± 138
BRU	2	1160–1183		
UA	12	539–1539	952	981 ± 87
AAU	6	105–595	227	292 ± 83

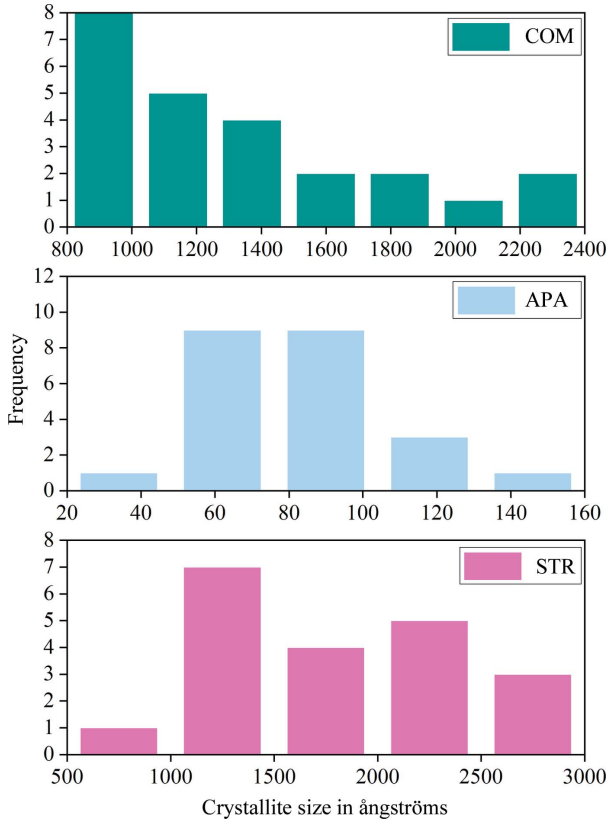

Figure 8
Histogram distributions of crystallite sizes for whewellite, weddellite and struvite.

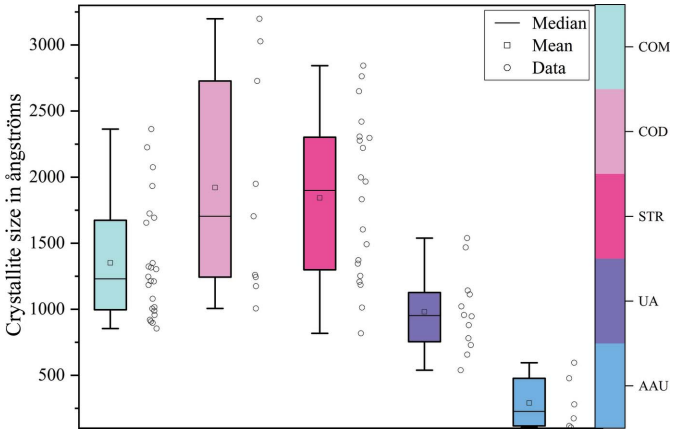

Figure 9
Box plots of crystallite sizes for whewellite, weddellite, struvite, uric acid and ammonium acid urate.

Table 3
Integral breadth (IB) and FWHM averaged crystallite sizes for selected samples.

Label	Phase	IB (Å)	FWHM (Å)
C1	UA	386	428
C7	UA	413	443
C8	STR	749	829
C12	STR	914	1109
C40	COM	636	690
C41	COM	710	799
C44	STR	657	734

the lowest due to the low crystallinity calculated for hydroxyapatite, which Mirković *et al.* (2020) recorded to be around 18%. The high percent crystallinity calculated for struvite and brushite, however, acts as the buffer for the phosphate group.

In reference to biological hydroxyapatite, Londoño-Restrepo *et al.* (2019) highlighted issues regarding reports of low crystallinity by the scientific community. In fact, their high-resolution transmission electron microscopy study revealed high atomic structural order for APA crystals from human, bovine and porcine bones. Londoño-Restrepo and co-workers measured bi-dimensional APA crystals to be 21 ± 8 nm long and 6 ± 2 nm wide for human bone and even smaller for the bovine and porcine samples. The ability to evaluate crystalline quality accurately using traditional XRD methods for apatite is tied to the difficulty in isolating the effects of inelastic scattering for nano-scaled crystallites. Whilst the present investigation has found 'low crystallinity' for apatite, we have also provided results of nanometric APA crystals in kidney stones based on 23 Rietveld refinements.

3.6. Clinical implications

Schubert (2006) assessed the compositions of more than 110 000 stones and published the frequencies of mineral components as 78% for COM, 43% COD, 33% APA, 10% UA, 6% STR, 1–2% BRU and 1% AAU. Here, we have reported lower frequencies of COM and COD and a significantly higher prevalence of all other phases amongst a small sample of 52 stones.

An excessive 42% of calculi contained struvite, which speaks of infection either as the origin of the stone or occurring at some point thereafter. Struvite stones are regarded as high risk for recurrence and sepsis (Gao *et al.*, 2020; Turk *et al.*, 2020). The higher the struvite content, the greater the recurrence risk (Nevo *et al.*, 2019). One study reported a strong correlation between mixed CaOx–struvite calculi and hypercalciuria in patients (Kristensen *et al.*, 1987), implicating infection as a secondary event to metabolically triggered CaOx urolithiasis. This is significant, as our phase correlation statistics have shown the unlikelihood of COM content in a struvite stone. Nevertheless, a few cases (C16, C19, C31, C38 and C45) detailed in Table 1 present a COM–STR combination. According to the literature, infection may be the secondary cause and a clinical investigation ought to include metabolic evaluation of the patient.

A considerable number of stones (19%) were revealed to comprise AAU. Although this phase is predominantly linked with infection, similarly to struvite (Tiselius, 2000; Chou *et al.*, 2012), associations have also been made with morbid obesity, recurrent uric acid stones, irritable bowel syndrome and laxative abuse (Soble *et al.*, 1999; Kuruma *et al.*, 2006; Lomas *et al.*, 2017). Kuruma *et al.* (2006) contemplated a need to distinguish between pure and mixed AAU stones as there were perceptible clinical differences between the two groups. They reported that 70% of the pure AAU group had history with laxative abuse, whilst mixed AAU stone formers were principally older men deemed as overweight. In the present work, AAU-containing stones were never pure but most often discovered with struvite (60%) and UA (60%), or with both phases 30% of the time. Infection seems innately related to AAU crystallization but it is doubtful that this is what actually initiated most stones. The key to this is the UA content, which suggests a metabolic origin, with a possible infection as the secondary promoter. A common thread of AAU surveys, though, is the regular appearance of serious co-morbidities in study participants. Lomas *et al.* (2017) found diabetes in 9% and chronic kidney disease in 11% of patients. Chou *et al.* (2012) gave figures of 60% for CKD and 12% for urothelial carcinoma and noted an elevated recurrence risk. In the light of this, AAU lithiasis represents a critical class of stone formers from this study that must be evaluated further.

Infection-related, uric acid and brushite-containing stones are all classed as high risk for recurrence by the European Association of Urology (Turk *et al.*, 2020). Furthermore, non-calcium stones are associated with reduced renal function (Chou *et al.*, 2011). This investigation has highlighted a substantial proportion of these high-risk constituent phases amongst a sample of stones from hospitals in Trinidad. Due to the limited sample size, additional research is required to confirm whether the trend persists for the larger population of stone patients in the country. Should this be the case, an investigation into specific risk factors for the local population would be necessary for preventative care.

3.7. Benefits and outlook

Analysis of powder XRD data with a Rietveld-based approach not only provides a means for quantitative estimation of crystalline phases but often facilitates a qualitative assessment. In practice, minority yet critical phases had been missed in the phase identification step, with small peaks being overlooked as 'impurity' peaks prior to Rietveld analysis. The calculation of an entire profile pattern from the already-known phases would then allow us to correct such oversights. For example, minor amounts of apatite were overshadowed by sharp peaks of other phases as in samples C9–C11, or the reverse scenario might occur whereby peak overlap of phases with small crystallite sizes masks normally well defined peaks of other minerals. Additionally, crowded diffractograms with three to four minerals sometimes concealed one of the components, like for struvite in C31 or whewellite in C16. The subsequent classification of stones according to phase fraction estimates is made more accurate by whole-powder-pattern fitting.

A further benefit of the Rietveld method for kidney stone analysis is the deeper insight granted by the characterization of structure and microstructure of mineral components. Shapur *et al.* (2012) proposed that, for whewellite and apatite, crystallite size is related to the eventual volume of the macroscopic stone. In their study, smaller crystallites were associated with higher stone burdens, whereas larger crystallites were associated with smaller stones. Shapur and co-workers suggested that this may be useful for predicting the potential for an obstructive stone in a patient. In the biological context, crystallite size is a parameter for renal cytotoxicity. It has been shown that smaller whewellite, weddellite and apatite crystals result in higher renal cell death (Sun, Gan & Ouyang, 2015; Sun, Ouyang *et al.*, 2015; Sun *et al.*, 2020; Bazin *et al.*, 2021). Daudon *et al.* (2016) carried out neutron powder diffraction analysis and discovered significant differences in uric acid crystallite size for non-diabetic males and females, but no variation in size between diabetics. From findings such as these, it is clear that the role of crystallite size should be more thoroughly assessed for its biological and medical implications.

Significant progress has been made in urolithiasis research within the past four decades, yet there are still a few fundamental gaps in knowledge, for example with regard to mechanistic theories of crystal growth and aggregation, modulator macromolecules, and the role of trace elements in stone formation (Khan & Kok, 2004; Aggarwal *et al.*, 2013; Giannossi *et al.*, 2013; Singh & Rai, 2014; Ramaswamy *et al.*, 2015; Rodgers, 2017, 2019). Increased structural knowledge of biogenic crystalline materials could prove helpful to our understanding (Izatulina & Yelnikov, 2008). Variation in unit-cell parameters signals changes at the atomic and/or microscopic level indicative of the crystal growth and stone formation process. For instance, a high degree of carbonation in hydroxyapatite stones is affiliated to bacterial origin (Carpentier *et al.*, 2009). As apatite is well studied for its applications, the relationship between incorporation of carbonate ions in the structure and the distance parameters a and c is established (Ren *et al.*, 2013). For weddellite, Izatulina *et al.* (2014) found a linear relationship between the unit-cell parameter a and the zeolitic water contained in its structure. More revelations such as these may be revealed with larger-scaled crystallographic investigations into kidney stone materials.

The current investigation has generated unit-cell parameter and crystallite size data for the most common kidney stone phases from PXRD Rietveld data. There are too few studies which have stepped in this direction (Izatulina & Yelnikov, 2008; Ghosh *et al.*, 2009, 2014; Mukherjee, 2014; Chatterjee *et al.*, 2015, 2018; Cruz-May *et al.*, 2021). Considering the challenges of multiphasic refinement, only one other study thus far has published data for more than 30 stones (Chatterjee *et al.*, 2018). More studies would be vital for affirmation of structural and microstructural data for classic kidney stones and finding any trends which may prove clinically relevant.

4. Conclusions

Stone analysis for the determination of crystalline constituents is a crucial step in risk assessment for recurrence prevention of stone disease. A powder X-ray diffraction study with Rietveld analysis was employed for a quantitative, structural and microstructural assessment of the compositional crystalline phases in 46 urinary tract calculi.

The refined crystallite sizes ranged from 85 to 236 nm for COM ($N = 24$), 101 to 320 nm for COD ($N = 9$), 3 to 15 nm for APA ($N = 23$), 82 to 284 nm for STR ($N = 20$), 116 to 118 nm for BRU ($N = 2$), 54 to 154 nm for UA ($N = 12$) and 11 to 60 nm for AAU ($N = 6$). The phase weight fractions allowed the classification of the sample set as 36.5% phosphates, 34.6% oxalates, 15.4% mixed stones and 13.5% uric acid/urates.

The study has found an elevated frequency in the appearance of high-risk phases such as struvite (42%), uric acid (23%), ammonium acid urate (19%) and brushite (6%), indicating the need for prophylactic intervention in study patients.

The application of the Rietveld method is beneficial for enhanced accuracy through whole-pattern fitting, but also for establishing structural values for crystalline phases which may be helpful for understanding stone growth processes.

Acknowledgements

The authors thank Mr Adrian Gayah and Ms Sadira Khan of the Materials Sciences Laboratory at the University of the West Indies for their technical assistance.

References

Aggarwal, K. P., Narula, S., Kakkar, M. & Tandon, C. (2013). *Biomed. Res. Int.* **2013**, 292953.
Al-Mamari, S. A. (2017). *Complications of Urolithiasis*, pp. 121–129. Heidelberg: Springer.
Basiri, A., Taheri, M. & Taheri, F. (2012). *Urol. J.* **9**, 445–454.
Bazin, D., André, G., Weil, R., Matzen, G., Emmanuel, V., Carpentier, X. & Daudon, M. (2012). *Urology*, **79**, 786–790.
Bazin, D., Chappard, C., Combes, C., Carpentier, X., Rouzière, S., André, G., Matzen, G., Allix, M., Thiaudière, D., Reguer, S., Jungers, P. & Daudon, M. (2009). *Osteoporos. Int.* **20**, 1065–1075.
Bazin, D., Frochot, V., Haymann, J.-P., Letavernier, E. & Daudon, M. (2021). *C. R. Chim.* **24**(S2), 96.
Breslau, N. A., Brinkley, L., Hill, K. D. & Pak, C. Y. C. (1988). *J. Clin. Endocrinol. Metab.* **66**, 140–146.
Carpentier, X., Daudon, M., Traxer, O., Jungers, P., Mazouyes, A., Matzen, G., Véron, E. & Bazin, D. (2009). *Urology*, **73**, 968–975.
Chatterjee, P., Chakraborty, A. & Mukherjee, A. K. (2018). *Spectrochim. Acta A Mol. Biomol. Spectrosc.* **200**, 33–42.
Chatterjee, P., Pramanik, S. & Mukherjee, A. K. (2015). *J. Appl. Cryst.* **48**, 1794–1804.
Chou, Y.-H., Huang, C.-N., Li, W.-M., Huang, S.-P., Wu, W.-J., Tsai, C.-C., Chang, A.-W., Chen, S.-M., Lin, Y.-L. & Lin, Y.-P. (2012). *Kaohsiung J. Med. Sci.* **28**, 259–264.
Chou, Y.-H., Li, C.-C., Hsu, H., Chang, W.-C., Liu, C.-C., Li, W.-M., Ke, H.-L., Lee, M.-H., Liu, M.-E., Pan, S.-C. & Wang, H. S. (2011). *Kaohsiung J. Med. Sci.* **27**, 264–267.
Cloutier, J., Villa, L., Traxer, O. & Daudon, M. (2015). *World J. Urol.* **33**, 157–169.
Coe, F. L., Parks, J. H. & Asplin, J. R. (1992). *N. Engl. J. Med.* **327**, 1141–1152.
Cruz-May, T. N., Herrera, A., Rodríguez-Hernández, J., Basulto-Martínez, M., Flores-Tapia, J. P. & Quintana, P. (2021). *J. Mol. Struct.* **1235**, 130267.
Daudon, M., Bazin, D., André, G., Jungers, P., Cousson, A., Chevallier, P., Véron, E. & Matzen, G. (2009). *J. Appl. Cryst.* **42**, 109–115.
Daudon, M., Dessombz, A., Frochot, V., Letavernier, E., Haymann, J.-P., Jungers, P. & Bazin, D. (2016). *C. R. Chim.* **19**, 1470–1491.
Daudon, M. & Jungers, P. (2012). *Urolithiasis: Basic Science and Clinical Practice*, edited by J. T. Talati, H.-G. Tiselius, D. M. Albala & Z. Ye, pp. 113–140. Heidelberg: Springer.
Daudon, M., Jungers, P. & Bazin, D. (2008). *AIP Conf. Proc.* **1049**, 199–215.
Daudon, M., Letavernier, E., Weil, R., Véron, E., Matzen, G., André, G. & Bazin, D. (2016). *C. R. Chim.* **19**, 1527–1534.
Evan, A. P., Lingeman, J. E., Coe, F. L., Shao, Y., Parks, J. H., Bledsoe, S. B., Phillips, C. L., Bonsib, S., Worcester, E. M., Sommer, A. J., Kim, S. A. M. C., Tinmouth, W. W. & Grynpas, M. (2005). *Kidney Int.* **67**, 576–591.
Finlayson, B. (1978). *Kidney Int.* **13**, 344–360.
Friedel, P., Bergmann, J., Kleeberg, R. & Schubert, G. (2015). *Z. Cryst. Suppl.* **23**, 517–522.
Gao, X., Lu, C., Xie, F., Li, L., Liu, M., Fang, Z., Wang, Z., Ming, S., Dong, H., Shen, R., Sun, Y., Peng, Y. & Gao, X. (2020). *World J. Urol.* **38**, 219–229.
Ghosh, S., Basu, S., Chakraborty, S. & Mukherjee, A. K. (2009). *J. Appl. Cryst.* **42**, 629–635.
Ghosh, S., Bhattacharya, A., Chatterjee, P. & Mukherjee, A. K. (2014). *Z. Kristallogr. Cryst. Mater.* **229**, 451–458.
Giannossi, M. L., Mongelli, G., Tateo, F. & Summa, V. (2012). *J. X-ray Sci. Technol.* **20**, 175–186.
Giannossi, M. L., Summa, V. & Mongelli, G. (2013). *J. Trace Elem. Med. Biol.* **27**, 91–97.
Gillen, D. L., Worcester, E. M. & Coe, F. L. (2005). *Kidney Int.* **67**, 685–690.
Grases, F., Costa-Bauzá, A. & García-Ferragut, L. (1998). *Adv. Colloid Interface Sci.* **74**, 169–194.
Grases, F., Costa-Bauzá, A., Königsberger, E. & Königsberger, L.-C. (2000). *Int. Urol. Nephrol.* **32**, 19–27.
Gražulis, S., Chateigner, D., Downs, R. T., Yokochi, A. F. T., Quirós, M., Lutterotti, L., Manakova, E., Butkus, J., Moeck, P. & Le Bail, A. (2009). *J. Appl. Cryst.* **42**, 726–729.
He, J.-Y., Deng, S.-P. & Ouyang, J.-M. (2010). *IEEE Trans. Nanobiosci.* **9**, 156–163.
Hess, B. (1990). *Urol. Res.* **18**, S45–S48.
Hesse, A., Brändle, E., Wilbert, D., Köhrmann, K.-U. & Alken, P. (2003). *Eur. Urol.* **44**, 709–713.
Hill, R. J. & Howard, C. J. (1987). *J. Appl. Cryst.* **20**, 467–474.
Hossain, R. Z., Ogawa, Y., Hokama, S., Morozumi, M. & Hatano, T. (2003). *Int. J. Urol.* **10**, 411–415.
Izatulina, A., Gurzhiy, V. & Frank-Kamenetskaya, O. (2014). *Am. Mineral.* **99**, 2–7.
Izatulina, A. R., Gurzhiy, V. V., Krzhizhanovskaya, M. G., Kuz'mina, M. A., Leoni, M. & Frank-Kamenetskaya, O. V. (2018). *Cryst. Growth Des.* **18**, 5465–5478.
Izatulina, A. R. & Yelnikov, V. Y. (2008). *Minerals as Advanced Materials I*, edited by S. V. Krivovichev, pp. 231–239. Heidelberg: Springer.
Jamal, A. & Ramzan, A. (2004). *J. Coll. Phys. Surg. Pak.* **14**, 411–415.
Kartha, G., Calle, J. C., Marchini, G. S. & Monga, M. (2012). *Urol. Clin. North Am.* **40**, 135–147.
Keddis, M. T. & Rule, A. D. (2013). *Curr. Opin. Nephrol. Hypertens.* **22**, 390–396.
Keshavarzi, B., Yavar Ashayeri, N., Moore, F., Irani, D., Asadi, S., Zarasvandi, A. & Salari, M. (2016). *Minerals*, **6**, 131.
Khan, S. R. & Kok, D. J. (2004). *Front. Biosci.* **9**, 1450–1482.

Khan, S. R., Pearle, M. S., Robertson, W. G., Gambaro, G., Canales, B. K., Doizi, S., Traxer, O. & Tiselius, H.-G. (2016). *Nat. Rev. Dis. Primers*, **2**, 1–23.
Klee, L. W., Brito, C. G. & Lingeman, J. E. (1991). *J. Urol.* **145**, 715–718.
Kok, D. J., Papapoulos, S. E. & Bijvoet, O. L. M. (1990). *Kidney Int.* **37**, 51–56.
Kourambas, J., Aslan, P., Teh, C. L., Mathias, B. J. & Preminger, G. M. (2001). *J. Endourol.* **15**, 181–186.
Kristensen, C., Parks, J. H., Lindheimer, M. & Coe, F. L. (1987). *Kidney Int.* **32**, 749–753.
Kuruma, H., Arakawa, T., Kubo, S., Hyodo, T., Matsumoto, K., Satoh, T., Egawa, S. & Baba, S. (2006). *Int. J. Urol.* **13**, 498–501.
Le Bail, A., Cranswick, L. M. D. & Madsen, I. (2008). *Powder Diffraction: Theory and Practice.* Cambridge: Royal Society of Chemistry.
Lieske, J. C., de la Vega, L. S. P., Gettman, M. T., Slezak, J. M., Bergstralh, E. J., Melton, L. J. III & Leibson, C. L. (2006). *Am. J. Kidney Dis.* **48**, 897–904.
Liu, Y., Chen, Y., Liao, B., Luo, D., Wang, K., Li, H. & Zeng, G. (2018). *Asia. J. Urol.* **5**, 205–214.
Lomas, D. J., Jaeger, C. D. & Krambeck, A. E. (2017). *Urology*, **102**, 43–47.
Londoño-Restrepo, S. M., Jeronimo-Cruz, R., Millán-Malo, B. M., Rivera-Muñoz, E. M. & Rodriguez-García, M. E. (2019). *Sci. Rep.* **9**, 5915.
Lutterotti, L., Matthies, S. & Wenk, H. R. (1999). *IUCr Commission on Powder Diffraction Newsletter*, No. 21, pp. 14–15.
Ma, R., Luo, X., Li, Q. & Zhong, H. (2017). *Int. J. Surg.* **41**, 150–161.
Madore, F., Stampfer, M. J., Rimm, E. B. & Curhan, G. C. (1998). *Am. J. Hypertens.* **11**, 46–53.
Maurice-Estepa, L., Levillain, P., Lacour, B. & Daudon, M. (1999). *Scand. J. Urol. Nephrol.* **33**, 299–305.
Mirković, M., Dosen, A., Erić, S., Vulić, P., Matović, B. & Rosić, A. (2020). *Microchem. J.* **152**, 104429.
Moe, O. W. (2006). *Lancet*, **367**, 333–344.
Mosli, H. A., Mosli, H. H. & Kamal, W. K. (2013). *Res. Rep. Urol.* **5**, 11–15.
Mukherjee, A. K. (2014). *J. Indian Inst. Sci.* **94**, 35–44.
Nevo, A., Shahait, M., Shah, A., Jackman, S. & Averch, T. (2019). *Int. Urol. Nephrol.* **51**, 585–591.
Pak, C. Y. C. (1998). *Lancet*, **351**, 1797–1801.
Pfau, A. & Knauf, F. (2016). *Am. J. Kidney Dis.* **68**, 973–985.
Prezioso, D., Illiano, E., Piccinocchi, G., Cricelli, C., Piccinocchi, R., Saita, A., Micheli, C. & Trinchieri, A. (2014). *Arch. Ital. Urol. Androl.* **86**, 99–102.
Prywer, J. & Torzewska, A. (2010). *Cryst. Res. Technol.* **45**, 1283–1289.
Rahman, N. U., Meng, M. V. & Stoller, M. L. (2003). *Curr. Pharm. Des.* **9**, 975–981.
Ramaswamy, K., Killilea, D. W., Kapahi, P., Kahn, A. J., Chi, T. & Stoller, M. L. (2015). *Nat. Rev. Urol.* **12**, 543–557.
Ramello, A., Vitale, C. & Marangella, M. (2001). *J. Nephrol.* **13**, S45–S50.
Ren, F., Lu, X. & Leng, Y. (2013). *J. Mech. Behav. Biomed. Mater.* **26**, 59–67.
Rietveld, H. M. (1967). *Acta Cryst.* **22**, 151–152.
Rietveld, H. M. (1969). *J. Appl. Cryst.* **2**, 65–71.
Ringertz, H. (1966). *Acta Cryst.* **20**, 397–403.
Rodgers, A. L. (2017). *Urolithiasis*, **45**, 27–32.
Rodgers, A., Trinchieri, A., Ather, M. H. & Buchholz, N. (2019). *Urolithiasis*, **47**, 401–413.
Rule, A. D., Krambeck, A. E. & Lieske, J. C. (2011). *Clin. J. Am. Soc. Nephrol.* **6**, 2069–2075.
Sakhaee, K., Adams-Huet, B., Moe, O. W. & Pak, C. Y. C. (2002). *Kidney Int.* **62**, 971–979.
Schofield, P. F., Knight, K. S., Houwen, J. A. M. & Valsami-Jones, E. (2004). *Phys. Chem. Miner.* **31**, 606–624.
Schubert, G. (2006). *Urol. Res.* **34**, 146–150.
Shapur, N. K., Uvarov, V., Popov, I., Katz, R., Gofrit, O. N., Landau, E. H., Pode, D. & Duvdevani, M. (2012). *Urology*, **80**, 980–985.
Sharma, A. P. & Filler, G. (2010). *Indian J. Urol.* **26**, 516.
Shekarriz, B. & Stoller, M. L. (2002). *J. Urol.* **168**, 1307–1314.
Singh, V. K. & Rai, P. K. (2014). *Biophys. Rev.* **6**, 291–310.
Soble, J. J., Hamilton, B. D. & Streem, S. B. (1999). *J. Urol.* **161**, 869–873.
Stamatelou, K. K., Francis, M. E., Jones, C. A., Nyberg, L. M. Jr & Curhan, G. C. (2003). *Kidney Int.* **63**, 1817–1823.
Sudarsanan, K. & Young, R. A. (1969). *Acta Cryst.* B**25**, 1534–1543.
Sun, L.-M., Lin, C.-L., Chang, Y.-J., Liang, J.-A., Liu, S.-H., Sung, F.-C. & Kao, C.-H. (2013). *BJU Int.* **112**, 1150–1155.
Sun, X.-Y., Chen, J.-Y., Rao, C.-Y. & Ouyang, J.-M. (2020). *Int. J. Nanomed.* **15**, 5043–5060.
Sun, X. Y., Gan, Q. Z. & Ouyang, J. M. (2015). *Cell Death Discovery*, **1**, 1–8.
Sun, X.-Y., Ouyang, J.-M., Zhu, W.-Y., Li, Y.-B. & Gan, Q.-Z. (2015). *J. Mater. Chem. B*, **3**, 1864–1878.
Tang, X. & Lieske, J. C. (2014). *Curr. Opin. Nephrol. Hypertens.* **23**, 385–390.
Taylor, E. N., Stampfer, M. J. & Curhan, G. C. (2005). *JAMA*, **293**, 455–462.
Tazzoli, V. & Domeneghetti, C. (1980). *Am. Mineral.* **65**, 327–334.
Tiselius, H.-G. (2000). *Braz. J. Urol.* **26**, 452–462.
Turk, C., Neisius, A., Petřík, A., Seitz, C., Thomas, K. & Skolarikos, A. (2020). *European Association of Urology Guidelines*, 2020 ed., presented at the EAU Annual Congress, Amsterdam, 2020. http://uroweb.org/guideline/urolithiasis/. Arnhem: The European Association of Urology Guidelines Office.
Uvarov, V., Popov, I., Shapur, N., Abdin, T., Gofrit, O. N., Pode, D. & Duvdevani, M. (2011). *Environ. Geochem. Health*, **33**, 613–622.
Whitaker, A. & Jeffery, J. W. (1970). *Acta Cryst.* B**26**, 1429–1440.
Williams, R. E. (1963). *Br. J. Urol.* **35**, 416–437.
Yoshida, O., Terai, A., Ohkawa, T. & Okada, Y. (1999). *Kidney Int.* **56**, 1899–1904.